Stem Cell Reports
Article
ISSCR
OPEN ACCESS

Mthfd2 Modulates Mitochondrial Function and DNA Repair to Maintain the Pluripotency of Mouse Stem Cells

Liang Yue,[1,2] Yangli Pei,[1,3] Liang Zhong,[1,4] Henry Yang,[5] Yanliang Wang,[1] Wei Zhang,[1] Naixin Chen,[1] Qianqian Zhu,[1] Jie Gao,[1] Minglei Zhi,[1] Bingqiang Wen,[1] Shaopeng Zhang,[1] Jinzhu Xiang,[1] Qingqing Wei,[1] Hui Liang,[1] Suying Cao,[6] Huiqiang Lou,[1] Zhongzhou Chen,[1] and Jianyong Han[1,2,*]

[1]State Key Laboratory for Agrobiotechnology, College of Biological Sciences, China Agricultural University, Beijing 100193, China
[2]Advanced Innovation Center for Food Nutrition and Human Health, China Agricultural University, Beijing 100083, China
[3]School of Life Science and Engineering, Foshan University, Foshan, Guangdong 528231, China
[4]Hebei Provincial Key Laboratory of Basic Medicine for Diabetes, The Shijiazhuang Second Hospital, Shijiazhuang, Hebei 050051, China
[5]Cancer Science Institute of Singapore, National University of Singapore, Singapore 117599, Singapore
[6]Animal Science and Technology College, Beijing University of Agriculture, Beijing 102206, China
*Correspondence: hanjy@cau.edu.cn
https://doi.org/10.1016/j.stemcr.2020.06.018

SUMMARY

The pluripotency of stem cells determines their developmental potential. While the pluripotency states of pluripotent stem cells are variable and interconvertible, the mechanisms underlying the acquisition and maintenance of pluripotency remain largely elusive. Here, we identified that methylenetetrahydrofolate dehydrogenase (NAD^+-dependent), methenyltetrahydrofolate cyclohydrolase (*Mthfd2*) plays an essential role in maintaining embryonic stem cell pluripotency and promoting complete reprogramming of induced pluripotent stem cells. Mechanistically, in mitochondria, *Mthfd2* maintains the integrity of the mitochondrial respiratory chain and prevents mitochondrial dysfunction. In the nucleus, *Mthfd2* stabilizes the phosphorylation of EXO1 to support DNA end resection and promote homologous recombination repair. Our results revealed that *Mthfd2* is a dual-function factor in determining the pluripotency of pluripotent stem cells through both mitochondrial and nuclear pathways, ultimately ensuring safe application of pluripotent stem cells.

INTRODUCTION

Pluripotent stem cells (PSCs), including embryonic stem cells (ESCs) and induced pluripotent stem cells (iPSCs), can self-renew or potentially differentiate into all cell types, a phenomenon known as pluripotency (Evans and Kaufman, 1981; Takahashi and Yamanaka, 2006). PSCs hold great promise for basic biomedical research, the production of genetically modified animals, and future clinical applications. Distinct pluripotent states, termed naive and primed pluripotency, have been described (Nichols and Smith, 2009). Naive PSCs resemble the preimplantation embryo inner cell mass (Boroviak et al., 2015) while primed PSCs resemble postimplantation embryonic epiblasts (Tesar et al., 2007). These states are reversible and interconvertible. The pluripotency of PSCs is known to determine the fate of embryonic development, and high-quality PSCs can produce chimeras with high efficiency when they are introduced into a blastocyst (Huang et al., 2012) and can develop into viable offspring by tetraploid complementation (Zhao et al., 2009; Zhong et al., 2019). Understanding the molecular mechanisms that influence pluripotency acquisition and maintenance is key to advancing therapeutic applications of PSCs.

Cells produce ATP by exploiting glycolysis and oxidative phosphorylation (OXPHOS) in different proportions to obtain energy for survival. Somatic cell reprogramming resets cellular metabolism to a state of relatively high glycolysis and low OXPHOS (Folmes et al., 2011). PSCs in a naive state are highly oxidative compared with primed cells. The progression from naive to primed pluripotency is characterized by a metabolic shift from OXPHOS to glycolysis (Zhou et al., 2012), and resetting primed pluripotent cells to a naive state necessitates a reversal of the metabolic switch (Carbognin et al., 2016; Takashima et al., 2014). Mitochondria are essential organelles in all nucleated cells that function mainly to generate cellular ATP by OXPHOS via the electron transport chain (ETC, complexes I–IV) and ATP synthase (complex V). Primed PSCs maintain lower mitochondrial function than naive cells (Zhang et al., 2016). In addition, the mitochondrial membrane potential (Sukumar et al., 2016), ATP (Zhang et al., 2018), reactive oxygen species (ROS) (Ryu et al., 2015; Zhou et al., 2016), and mitochondrial dynamics (Khacho et al., 2016; Zhong et al., 2019) were reported as the key factors responsible for cell-fate changes. However, the factors that determine mitochondrial function in PSCs and their regulatory mechanism remain unclear.

Genetic lesions of either endogenous or exogenous origin are major threats to the function of PSCs (Weissbein et al., 2014; Yoshihara et al., 2017). PSCs rely on a very robust DNA damage response (DDR) to detect and control specific types of DNA damage. Once DNA damage is unresolvable, PSCs avoid the propagation of genetic lesions by undergoing regulated cell death (Desmarais et al., 2016; Liu et al., 2013) or losing pluripotency (Li et al., 2012; Lin

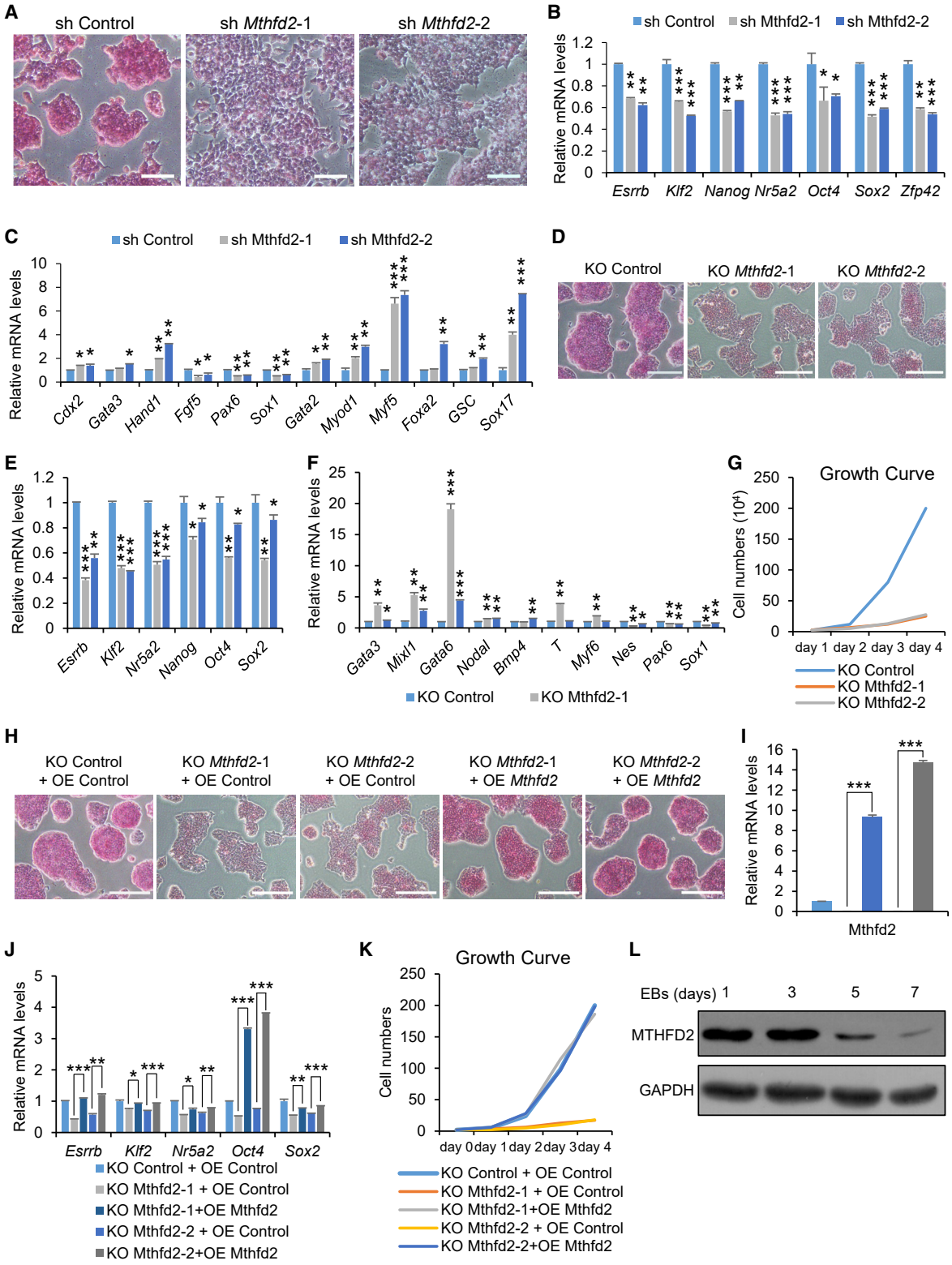

Figure 1. *Mthfd2* Is Important for mESCs to Maintain Self-Renewal

(A) Representative results of *Mthfd2* KD mESCs with AP staining. Scale bars, 100 μm.

(B and C) qRT-PCR analysis of mRNA levels of pluripotency marker genes (B) and lineage marker genes (C) in *Mthfd2* KD mESCs.

(legend continued on next page)

et al., 2005). Among all types of DNA lesions, DNA double-strand breaks (DSBs) are arguably the most dangerous (Jackson, 2002), and PSCs predominantly use homologous recombination (HR) to repair DSBs (Tichy et al., 2010). Failure of HR repair systems typically leads to severe consequences, such as genomic instability in cellular reprogramming (Gonzalez et al., 2013; Lee et al., 2016). Thus, efficacious DSB repair is a key element in the maintenance of high genomic integrity. However, the mechanisms that protect genomic integrity and the key regulators involved are not completely clear.

In this study, we identified methylenetetrahydrofolate dehydrogenase (NAD^+-dependent), methenyltetrahydrofolate cyclohydrolase (*Mthfd2*) as an important regulator of pluripotency in mouse PSCs. *Mthfd2* is a bifunctional enzyme with methylene dehydrogenase and cyclohydrolase activity involved in mitochondrial folate one-carbon metabolism (Tibbetts and Appling, 2010). *Mthfd2* plays an essential role in mouse embryonic development, because inactivation of this gene in mice was demonstrated to be lethal (Di Pietro et al., 2002). *MTHFD2* is markedly elevated in many cancers and positively correlated with poor prognosis in patients with cancer (Lin et al., 2018; Liu et al., 2014a; Pikman et al., 2016). In addition, *MTHFD2* is localized to the nucleus and affects proliferation independent of its enzymatic activity in cancer cells (Gustafsson Sheppard et al., 2015). However, the function of *Mthfd2* in PSCs has not been reported. Here, we demonstrated that *Mthfd2* mediates both mitochondrial function and DNA repair to determine the pluripotency state of PSCs, ultimately improving their potential use in various applications and their safety.

RESULTS

A Microarray Assay Identifies Putative New Pluripotency-Regulating Genes in iPSCs

We reanalyzed the microarray data from iPSCs of different quality initially generated in our laboratory and demonstrated the quality of the iPSCs based on their *in vitro* developmental potential (Han et al., 2010; Heng et al., 2010). High-quality iPSCs underwent germline transmission or produced mice derived completely from iPSCs by tetraploid complementation, while low-quality iPSCs produced only chimeras with a low coat color contribution. Candidate genes were selected based on their higher expression in high-quality iPSCs than in low-quality iPSCs (Table S1). Among these candidates, *Esrrb*, *Sall4*, *Gadd45a*, and *Rab32* were previously reported to be important for enhancing iPSC generation and modulating ESC pluripotency (Chen et al., 2016; Feng et al., 2009; Pei et al., 2015; Zhang et al., 2006). Besides, some new potential regulators such as *Mthfd2* were identified (Figure S1A).

Mthfd2 Plays a Key Role in Mouse ESCs to Maintain Self-Renewal

To validate the role of the candidate genes in regulating mouse ESC (mESC) self-renewal, we separately used short hairpin RNAs (shRNAs) to suppress the expression of candidate genes in E14 mESCs. *Mthfd2* knockdown (KD) resulted in loss of typical stem cell morphology (Figures S1B–S1D), with reduced alkaline phosphatase (AP) staining (Figure 1A). The expression of pluripotency marker genes was downregulated and that of lineage marker genes upregulated (Figures 1B, 1C, and S1E), showing that *Mthfd2* depletion results in differentiation of mESCs. We then knocked down *Mthfd2* in another G4 mESC line and found that the results were consistent with those in *Mthfd2* KD E14 mESCs (Figures S1F and S1G). Additionally, homozygous *Mthfd2* knockout (KO) mESCs were characterized by the loss of typical mESC morphology, abnormal expression of marker genes, and compromised cell proliferation (Figures 1D–1G and S1H). Forced expression of *Mthfd2* rescued the *Mthfd2* KO-induced differentiation and compromised cell proliferation (Figures 1H–1K). In addition, MTHFD2 protein expression was gradually silenced during the differentiation of mESCs into embryoid bodies (EBs) (Figure 1L). These results demonstrate a key role of *Mthfd2* in the maintenance of mESC self-renewal.

Mthfd2 Facilitates Mouse iPSC Induction

We used *Oct4*, *Sox2*, and *Klf4* (OSK) combined with various candidate factors, including *Mthfd2*, in a subsequent

(D) Representative results of *Mthfd2* KO mESCs with AP staining. Scale bars, 200 μm.
(E and F) qRT-PCR analysis of mRNA levels of pluripotency marker genes (E) and lineage marker genes (F) in *Mthfd2* KO mESCs.
(G) Representative growth curve of *Mthfd2* KO mESCs.
(H) Representative results of overexpressed (OE) *Mthfd2-Mthfd2* KO mESCs with AP staining. Scale bar, 200 μm.
(I and J) qRT-PCR analysis of mRNA levels of *Mthfd2* (I) and pluripotency marker genes (J) in OE *Mthfd2-Mthfd2* KO mESCs.
(K) Representative growth curve of OE *Mthfd2-Mthfd2* KO mESCs.
(L) Western blot analysis of the levels of the MTHFD2 protein during differentiation of mESCs. GAPDH was used as a loading control.
Data in (B), (C), (E), (F), (I) and (J) are pooled from three independent experiments (mean ± SD) relative to EF1-α and the control mESCs. *p < 0.05, **p < 0.01, ***p < 0.001 (Student's t test) compared with the control.
See also Figure S1.

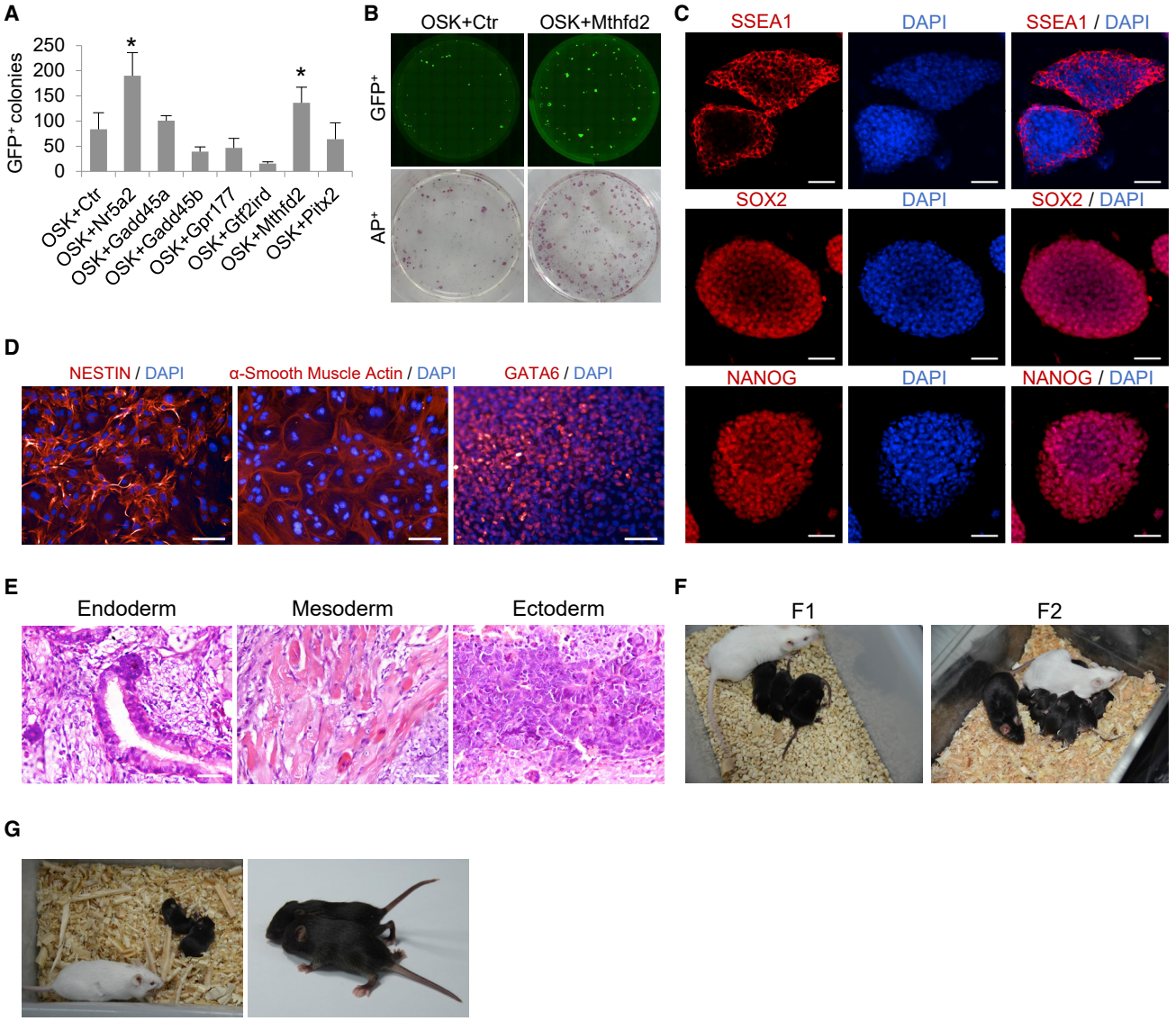

Figure 2. *Mthfd2* Promotes Complete Reprogramming of iPSCs

(A) The reprogramming efficiencies in KOSR medium. OSK + control (Ctr) cells were used as a control. Data are pooled from three independent experiments (mean ± SD). *$p < 0.05$, **$p < 0.01$, ***$p < 0.001$ (Student's t test) compared with the control.

(B) Full-well mosaic images of Oct4-GFP$^+$ cells and AP$^+$ colonies are shown for OSK+Ctr and OSKM2 iPSCs in KOSR medium.

(C) Immunofluorescence (IF) staining for pluripotency marker proteins in OSKM2 iPSCs. DAPI was used to indicate the nuclei. Scale bars, 100 μm.

(D) IF staining for GATA6 (endoderm), NESTIN (ectoderm), and α-smooth muscle actin (mesoderm) in EBs derived from OSKM2 iPSCs. DAPI was used to indicate the nuclei. Scale bars, 100 μm.

(E) H&E staining of teratomas derived from OSKM2 iPSCs. Scale bars, 100 μm.

(F) Representative images of chimeric mice (F1) and their offspring (F2).

(G) Live-born pups obtained from OSKM2 iPSCs were tested by tetraploid complementation.

See also Figure S2.

reprogramming assay (Takahashi and Yamanaka, 2006). Mouse embryonic fibroblasts (MEFs) expressing a green fluorescent protein (GFP) reporter driven by an *Oct4* promoter and enhancer (termed OG2 MEFs) were used for iPSC induction. To ensure the reliability of our results, we tested two culture conditions, serum + LIF (leukemia inhibitory factor) mESC medium and KOSR medium, the latter of which has been reported to enhance iPSC induction

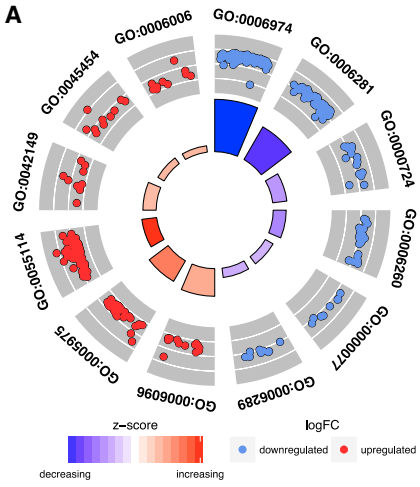

ID	Description
GO:0006974	cellular response to DNA damage stimulus
GO:0006281	DNA repair
GO:0000724	double−strand break repair via homologous recombination
GO:0006260	DNA replication
GO:0000077	DNA damage checkpoint
GO:0006289	nucleotide−excision repair
GO:0006096	glycolytic process
GO:0005975	carbohydrate metabolic process
GO:0055114	oxidation−reduction process
GO:0042149	cellular response to glucose starvation
GO:0045454	cell redox homeostasis
GO:0006006	glucose metabolic process

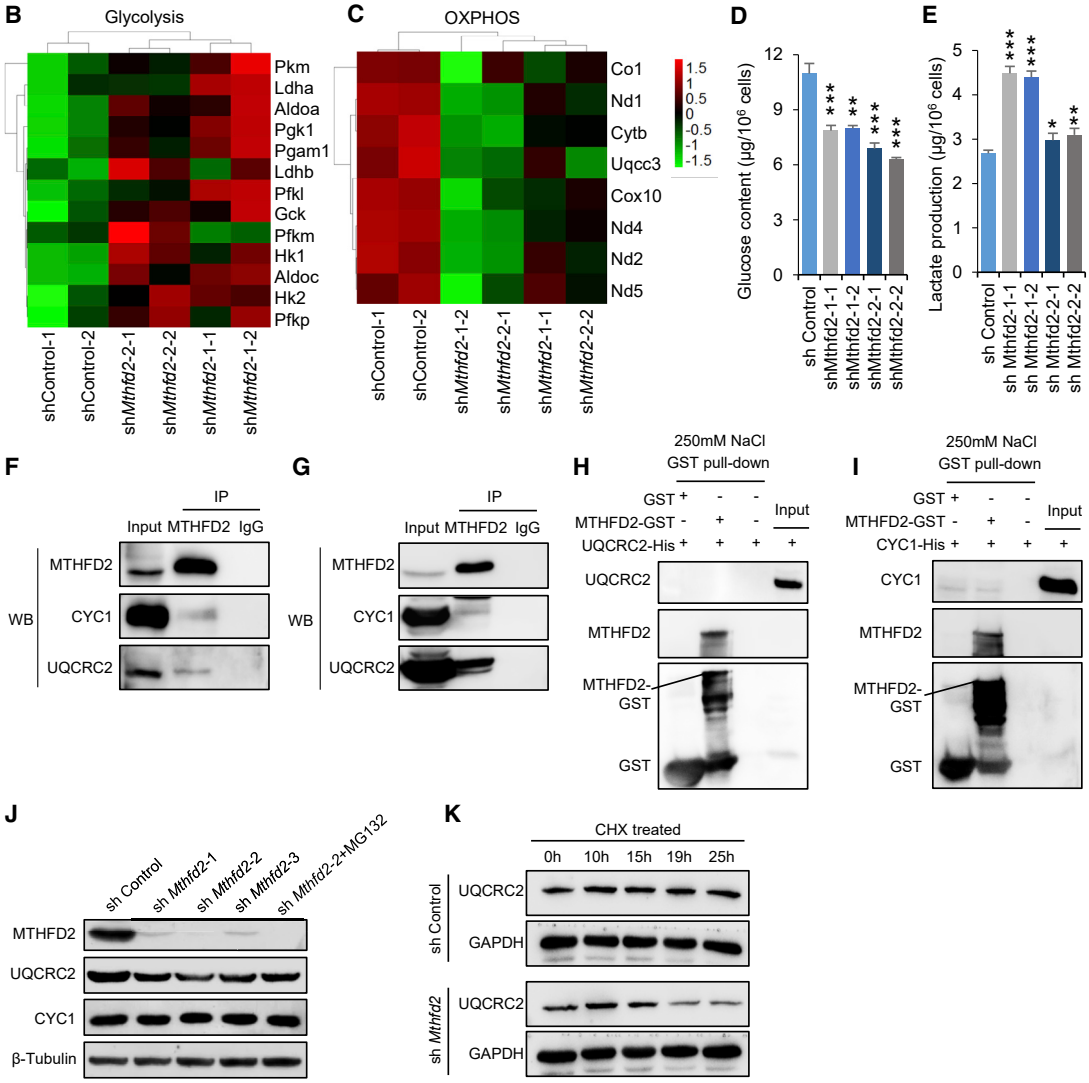

(legend on next page)

(Liu et al., 2014b). The number of Oct4-GFP$^+$ colonies generated by coinfection of *Mthfd2* and OSK was increased approximately 2-fold relative to that in control cells which coinfection of empty vector and OSK ($p < 0.05$) in both mESC medium (Figures S2A and S2B) and KOSR medium (Figures 2A and 2B). We used doxycycline-inducible MEFs expressing *Oct4*, *Sox2*, *Klf4*, and *c-Myc* (OSKC) reprogramming factor TF4 (Gao et al., 2013) for reprogramming to further confirm the *Mthfd2*-mediated improvements. The number of AP$^+$ colonies was increased in the *Mthfd2*-overexpressing group compared with that in the control group (Figures S2C and S2D) ($p < 0.05$). These results indicated that *Mthfd2* facilitates the induction of iPSCs.

Mthfd2 Improves the Quality of iPSCs

All iPSCs induced with *Mthfd2* (OSKM2 iPSCs) showed typical mESC-like morphology and expressed Oct4-driven GFP (Figure S2E). Exogenous retroviral expression of OSK and *Mthfd2* was silenced (Figure S2F), and the expression of pluripotency marker genes was similar in OSKM2 iPSCs and mESCs (Figure S2G). In addition, two master transcription factors (*Nanog* and *Sox2*) and the mESC-specific surface marker SSEA1 were expressed in OSKM2 iPSCs (Figure 2C).

We conducted EB and teratoma formation assays to assess the ability of OSKM2 iPSCs to differentiate *in vitro* and *in vivo*. The EBs and teratomas derived from OSKM2 iPSCs differentiated into cells of all three germ layers (Figures 2D and 2E). Furthermore, the developmental potential of OSKM2 iPSCs *in vivo* was tested via 8-cell embryo injection (Xiang et al., 2018), and chimeric mice derived almost completely from iPSCs were produced and had the ability of germline transmission (Figure 2F). Next, we tested the developmental potential of OSKM2 iPSCs *in vivo* by tetraploid complementation (Zhao et al., 2009). Remarkably, OSKM2 iPSCs gave rise to viable all-iPSC-derived pups (Figure 2G) with higher efficiency than control OSKC iPSCs (Figure S2H). Collectively, these results indicated that *Mthfd2* improves the quality of iPSCs.

Mthfd2 Depletion Shifts Glucose Metabolism from OXPHOS to Glycolysis in mESCs

MTHFD2 was reported to be an important enzyme in mitochondrial one-carbon metabolism (Tibbetts and Appling, 2010). Two MTHFD2-specific inhibitors, MIN and NIT (Asai et al., 2018), were used to inhibit MTHFD2 enzymatic activity in mESCs. Both MIN- and MIT-treated mESCs (MI-mESCs) maintained typical stem cell morphology and pluripotency-associated marker gene expression (Figures S3A–S3C). Therefore, we speculated that the MTHFD2 has non-enzymatic functions in mESCs. To characterize the global function of *Mthfd2* in mESCs, we analyzed changes in the transcriptome due to suppression of *Mthfd2* (Figure S3D and Table S2). Among the differentially expressed genes (DEGs), pluripotency-associated genes were downregulated in *Mthfd2* KD mESCs (Figure S3E). Interestingly, gene ontology (GO) terms such as glycolytic process were among the top ten terms enriched in upregulated genes (Figure S3F), and additional GO terms associated with carbohydrate metabolism were among the terms enriched in upregulated genes ($p < 0.05$) (Figure 3A). Glucose metabolism is a complex and dynamic process and is the most potent modulator of PSC pluripotency states and cell-fate changes (Carbognin et al., 2016; Shyh-Chang and Daley, 2015; Zhou et al., 2012). Subsequently, we evaluated whether the cellular glucose metabolism state was altered in *Mthfd2* KD mESCs. Among the DEGs, the levels of key glycolytic genes were increased and those of some key OXPHOS genes were decreased in *Mthfd2* KD mESCs (Figures 3B and 3C). Lower intracellular glucose levels and higher intracellular lactate levels were detected in *Mthfd2* KD cells than in control cells (Figures 3D and 3E), indicating increased consumption of glucose and production of lactate in *Mthfd2* KD mESCs. Therefore, *Mthfd2* depletion shifts glucose metabolism from OXPHOS to glycolysis in mESCs.

MTHFD2 Interacts with Mitochondrial ETC Complex III in Mitochondria

To understand the mechanism by which *Mthfd2* functions in mESCs, we used an immunoprecipitation and mass

Figure 3. MTHFD2 Interacts with Complex III to Regulate Glucose Metabolism in mESCs

(A) Summary of enriched GO terms that were potently upregulated and downregulated by *Mthfd2*. $p < 0.05$. For details, see Table S2.

(B and C) Heatmap of DEGs about glycolysis (B) and OXPHOS (C) between control mESCs and *Mthfd2* KD mESCs.

(D and E) Examination of intracellular glucose levels (D) and lactate levels (E) in *Mthfd2* KD mESCs. Data are pooled from three independent experiments (mean ± SD). *$p < 0.05$, **$p < 0.01$, ***$p < 0.001$ (Student's t test) compared with the control.

(F and G) CoIP results showing the specific interactions between endogenous MTHFD2 and both UQCRC2 and CYC1 in mESCs (F) and in the cytoplasm fraction of mESCs (G).

(H and I) GST pull-down assays for interaction between UQCRC2-His (H), CYC1-His (I), and MTHFD2-GST fusion proteins at 250 mM NaCl containing GST binding buffer.

(J) Western blot analysis of the levels of the UQCRC2 and CYC1 proteins in *Mthfd2* KD mESCs. β-Tubulin was used as a loading control.

(K) Western blot analysis of the levels of UQCRC2 protein in *Mthfd2* KD mESCs at indicated times post cycloheximide (CHX) treatment. GAPDH was used as a loading control.

See also Figures S3–S5.

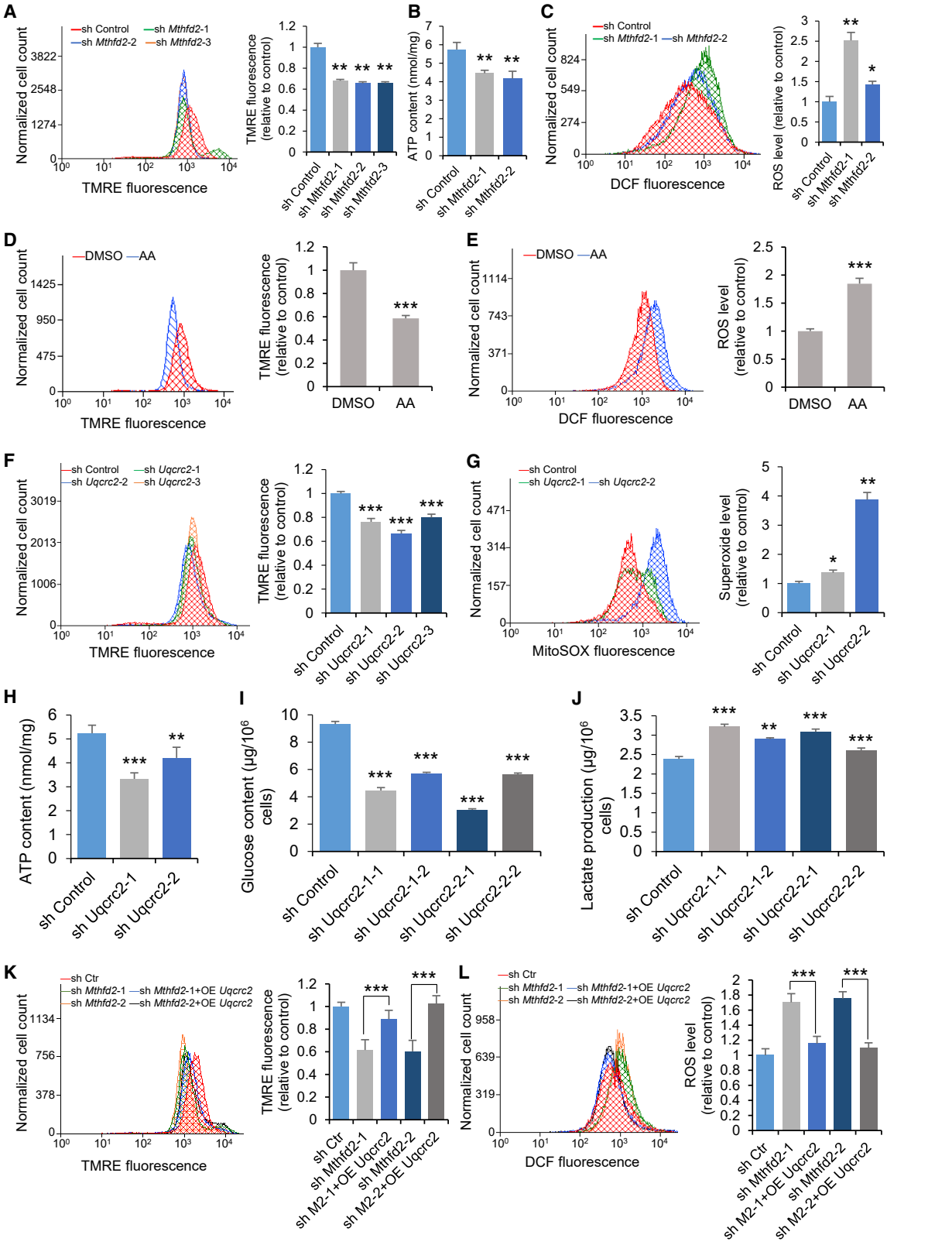

(legend on next page)

spectrometry (IP-MS) assay to search for proteins that interact with MTHFD2. MTHFD2 was localized to both the nucleus and mitochondria in mESCs (Figures S4A and S4B), and its function in mESCs, particularly in the nucleus, remains unknown. Hence, we separated nuclear and cytoplasmic fractions from Mthfd2-FLAG mESCs and subjected them to IP-MS (Figures S4C–S4F).

Among the identified MTHFD2 partners were the complex III members UQCRC2 and CYC1 (Figure S4G and Table S3). Complex III is a component of the mitochondrial ETC, via which OXPHOS is mediated to generate ATP in eukaryotic cells (Hatefi, 1985; Mitchell, 1975). Given the upregulation of glycolysis in *Mthfd2* KD mESCs, the interaction between MTHFD2 and complex III was particularly interesting. First, the interaction between FLAG-tagged MTHFD2 and hemagglutinin (HA)-tagged UQCRC2 was verified in E14 mESCs by reciprocal coimmunoprecipitation (coIP) experiments (Figure S5A). The specific interactions between endogenously expressed MTHFD2 and both UQCRC2 and CYC1 were then verified in E14 mESCs (Figure 3F). We further verified that MTHFD2 formed protein complexes with UQCRC2 and CYC1 in the cytoplasmic fraction (Figure 3G). To address the questions of whether the interactions between MTHFD2 and those proteins were direct, we conducted glutathione S-transferase (GST) pull-down assays using recombinant proteins. No direct interaction between MTHFD2-GST and either UQCRC2-His or CYC1-His was detected (Figures 3H and 3I). Thus, these results provide evidence for an indirect interaction between MTHFD2 and complex III in mitochondria of mESCs.

The protein level of UQCRC2 were reduced in *Mthfd2* KD mESCs compared with control mESCs (Figure S5B) but did not differ between MI-mESCs and control mESCs (Figure S5C). Treatment with a 26S proteasome inhibitor, MG132, efficiently prevented the *Mthfd2* depletion-induced reduction in UQCRC2 expression (Figure 3J). By treating cells with the protein synthesis inhibitor cycloheximide, we found that the half-life of UQCRC2 was considerably shortened upon depletion of *Mthfd2* (Figure 3K). Thus, *Mthfd2* might play a role in maintaining the stability of the UQCRC2 protein.

Mthfd2 Deficiency Induces Mitochondrial Dysfunction by Regulating the Activity of Complex III

The main function of complex III is to transfer electrons between ubiquinol and cytochrome *c*, thus generating an electrochemical potential that drives ATP synthesis (Crofts, 2004). In addition, complex III is the major site of ROS generation (Chen et al., 2003). The mitochondrial membrane potential (MMP) and ATP production were decreased (Figures 4A and 4B) and cellular ROS levels were increased in *Mthfd2* KD mESCs (Figure 4C). These effects are consistent with those observed in cells treated with antimycin A (a complex III inhibitor), which impairs mitochondrial function (Figures 4D and 4E), and indicated that *Mthfd2* deficiency induces mitochondrial dysfunction in mESCs.

The mitochondrial dysfunction induced by *Mthfd2* depletion resembled the phenotype observed in cells with *Uqcrc2* deficiency, which leads to complex III deficiency (Aguilera-Aguirre et al., 2009; Miyake et al., 2013). *Uqcrc2* KD cells exhibited reduced MMP and ATP production, increased levels of superoxide (a major ROS generated in mitochondria), and a shift of glucose metabolism to glycolysis (Figures 4F–4J). Moreover, forced expression of *Uqcrc2* effectively rescued the *Mthfd2* KD-induced changes in the MMP (Figure 4K) and the cellular ROS level (Figure 4L). In addition, the cellular ROS level (Figure S5D) and the MMP (Figure S5E) did not differ between MI-mESCs and control mESCs. Therefore, *Mthfd2* depletion induces mitochondrial dysfunction through inhibition of complex III activity caused by a decrease in UQCRC2 expression.

Mthfd2 Depletion Hinders DNA Repair in mESCs

In addition to GO terms related to glycolysis, GO terms such as DNA repair were among the top ten terms

Figure 4. *Mthfd2* Deficiency Induces Mitochondrial Dysfunction by Reducing *Uqcrc2* Expression

(A) Measurements of the mitochondrial membrane potential (MMP) in *Mthfd2* KD mESCs using tetramethylrhodamine methyl ester (TMRE).
(B) Total ATP levels in *Mthfd2* KD mESCs.
(C) Flow-cytometry analysis of ROS levels in *Mthfd2* KD mESCs.
(D) Measurements of the MMP in antimycin A-treated mESCs (AA-mESCs) using TMRE.
(E) Flow-cytometry analysis of ROS levels in AA-mESCs.
(F) Measurements of the MMP in *Uqcrc2* KD mESCs using TMRE.
(G) Flow-cytometry analysis of superoxide levels in *Uqcrc2* KD mESCs.
(H) Total ATP levels in *Uqcrc2* KD mESCs.
(I and J) Examination of intracellular glucose levels (I) and lactate levels (J) in *Uqcrc2* KD mESCs.
(K) Measurements of the MMP in OE *Uqcrc2-Mthfd2* KD mESCs using TMRE.
(L) Flow-cytometry analysis of ROS levels in OE *Uqcrc2-Mthfd2* KD mESCs.
All data are pooled from three independent experiments (mean ± SD). *$p < 0.05$, **$p < 0.01$, ***$p < 0.001$ (Student's t test) compared with the control. A representative histogram (left) and quantification of the mean fluorescence intensity (right) are presented for (A), (C) to (G), (K), and (L). See also Figure S5.

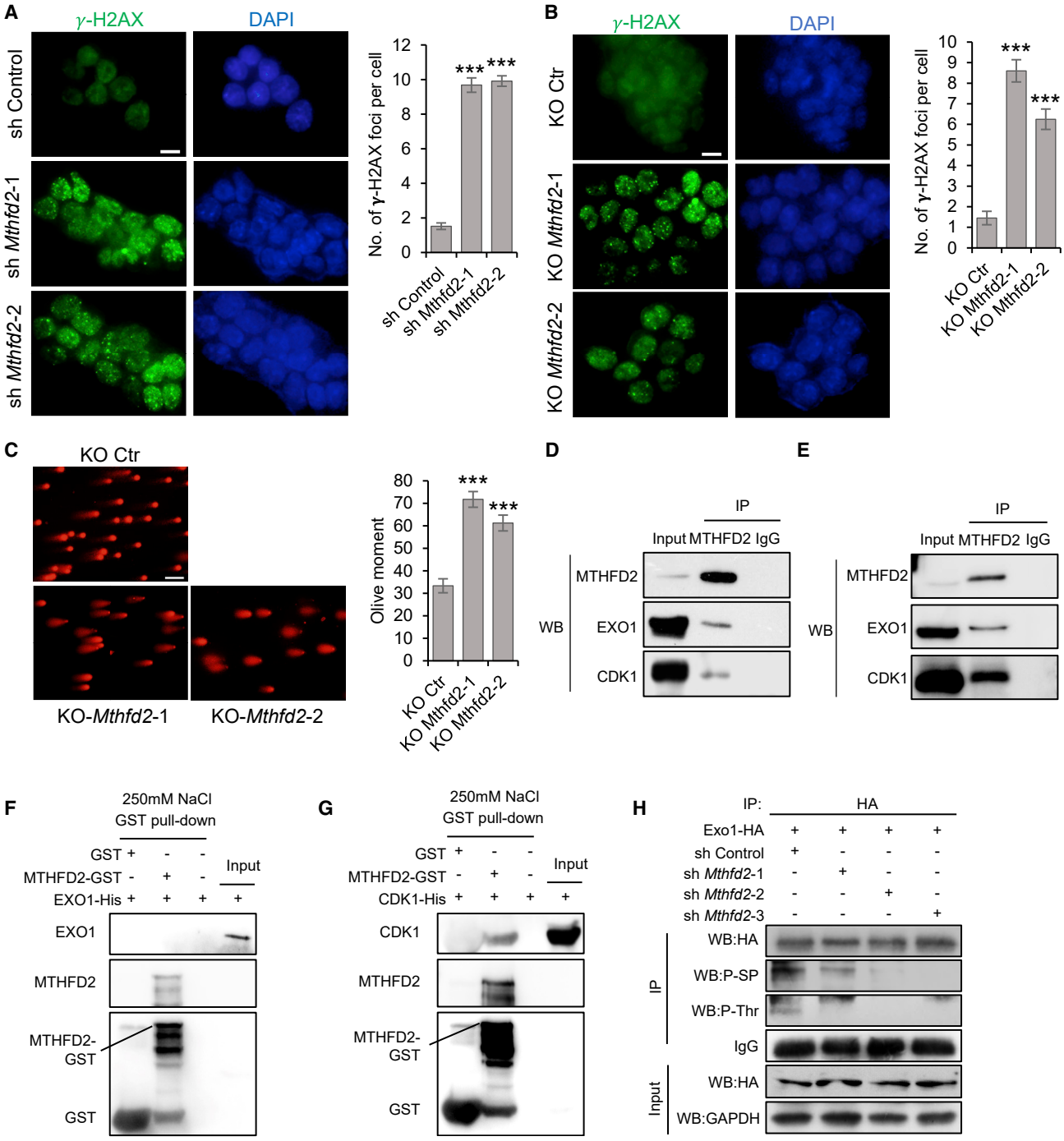

Figure 5. MTHFD2 Interacts with CDK1 and EXO1 to Regulate DNA Damage Level in mESCs

(A and B) IF staining for γ-H2AX in *Mthfd2* KD mESCs (A) *and Mthfd2* KO mESCs (B). Representative images (left) and quantification of the average number of γ-H2AX foci per cell (right) (n = 50 nuclei) are shown. DAPI was used to indicate the nuclei. Scale bar, 10 μm.

(C) DNA damage levels of *Mthfd2* KO mESCs were evaluated by the comet assay. Representative images (left) and quantification of the mean olive tail moment (right) (n = 50 nuclei) are shown. Scale bar, 100 μm.

(D and E) CoIP results showing the specific interactions between endogenous MTHFD2 and both CDK1 and EXO1 in mESCs (D) and in the nuclear fraction of mESCs (E).

(legend continued on next page)

enriched in downregulated genes (Figure S6A), and additional terms such as double-strand break repair via HR were enriched in downregulated genes ($p < 0.05$) (Figure 3A). PSCs rely on a very robust DNA repair response to control DNA damage, and if DNA damage is unresolvable, PSCs prevent the propagation of genetic lesions by undergoing regulated cell death (Liu et al., 2013) or losing pluripotency (Li et al., 2012; Lin et al., 2005). Therefore, we examined whether *Mthfd2* deficiency altered DNA damage levels in mESCs. Among the DEGs, DNA repair-associated genes exhibited decreased expression in *Mthfd2* KD mESCs (Figure S6B). Phosphorylation of H2AX (termed γ-H2AX) is one of the earliest events to occur following DNA DSB induction and is critical for protecting the genome from DSBs (Rogakou et al., 1998). Interestingly, the number of γ-H2AX foci increased substantially in *Mthfd2* KD mESCs (Figure 5A) and *Mthfd2* KO mESCs (Figure 5B) with increased passaging. The increase in DNA damage in *Mthfd2* KO mESCs was further validated by comet assay, a method that measures the extent of DNA damage on a single-cell basis (Figure 5C). These increases suggested that DNA damage accumulates following *Mthfd2* depletion.

MTHFD2 Interacts with CDK1 and EXO1 in the Nucleus

Under normal conditions, PSCs accurately repair DSBs mostly through the HR pathway (Tichy et al., 2010). EXO1 and CDK1, which play key roles in DNA HR repair (Tomimatsu et al., 2014), were detected among the identified MTHFD2 partners (Figure S4G and Table S3). Thus, we explored the interactions between MTHFD2 and both EXO1 and CDK1. The interactions between endogenously expressed MTHFD2 and both CDK1 and EXO1 were confirmed by coIP experiments (Figure 5D). We further verified that MTHFD2 interacts with both EXO1 and CDK1 in the nuclear fraction (Figures 5E and S6C). Moreover, a direct interaction between MTHFD2-GST and CDK1-His was detected by GST pull-down assays (Figures 5F and 5G). These results provide evidence for the interaction of CDK1 and EXO1 with MTHFD2 in the nucleus of mESCs. In addition, the interactions between MTHFD2 and UQCRC2, CYC1, CDK1, and EXO1 remained detectable in MI-mESCs (Figure S6D), emphasizing that the MTHFD2's interactions are not affected by its enzymatic activity.

During HR repair, EXO1 is primed to function in resection by CDK-mediated phosphorylation (Tomimatsu et al., 2014). We assessed the level of CDK1-induced EXO1 phosphorylation in *Mthfd2* KD mESCs. EXO1 phosphorylation was significantly reduced in *Mthfd2* KD mESCs compared with that in control mESCs (Figure 5H). Collectively, these results indicate that *Mthfd2* plays an important role in maintaining the phosphorylation of EXO1 in mESCs.

Mthfd2 Modulates HR Repair by Regulating EXO1 Phosphorylation

To understand whether the increased DNA damage in *Mthfd2* KD mESCs was caused by defects in DNA repair, we quantified and compared γ-H2AX foci formation after treatment with camptothecin (CPT), which induces DSBs (Hsiang et al., 1989). A significant reduction in DNA repair efficiency was observed in *Mthfd2* KD mESCs (Figures 6A, 6B, S6E, and S6F) and *Exo1* KD mESCs (Figures 6C, 6D, and S6G) after CPT treatment, consistent with a previous report that *Exo1* deletion impairs HR repair (Schaetzlein et al., 2007). This pattern was consistent with that observed in cells treated with RO-3306 (a specific CDK1 inhibitor), which hinders DNA repair and increases DNA damage (Figures 6E and 6F). Moreover, the comet assay results showed that forced expression of *Cdk1* effectively rescued the *Mthfd2* KD-induced impairment in DNA repair (Figure 6G). However, DNA damage level did not differ between MI-mESCs and control mESCs (Figures S6H and S6I), highlighting a key role of EXO1 phosphorylation in *Mthfd2*-mediated functions during DNA repair. Moreover, *Mthfd2* KD mESCs exhibited fewer Rad51 foci, a key component of HR repair, than control cells after CPT treatment, suggesting attenuation of HR repair (Figures 6H and 6I). These results revealed that *Mthfd2* regulates EXO1 phosphorylation by affecting the kinase activity of CDK1 to modulate HR repair and protect genomic integrity.

Mthfd2 Regulates Pluripotency of PSCs by Mediating Both Mitochondrial Function and HR Repair

To further confirm whether *Mthfd2* regulates pluripotency of PSCs by mediating both mitochondrial function and HR repair, on the one hand we transfected mESCs with two sets of shRNAs against *Uqcrc2* or *Exo1*. Depletion of *Uqcrc2* or *Exo1* led to the differentiation of mESCs (Figures S7A–S7G). Moreover, cosuppression of *Uqcrc2* and *Exo1* led to the differentiation of mESCs with reduced AP staining (Figures 7A and 7B), and the expression pattern of marker genes in these cells was more consistent with that in

(F and G) GST pull-down assays for interaction between EXO1-His (F), CDK1-His (G), and MTHFD2-GST fusion proteins at 250 mM NaCl containing GST binding buffer.

(H) Representative results showing the EXO1 phosphorylation status in *Mthfd2* KD mESCs.

Data in (A) to (C) are pooled from three independent experiments (mean ± SEM). *$p < 0.05$, **$p < 0.01$, ***$p < 0.001$ (Student's t test) compared with the control. See also Figure S6.

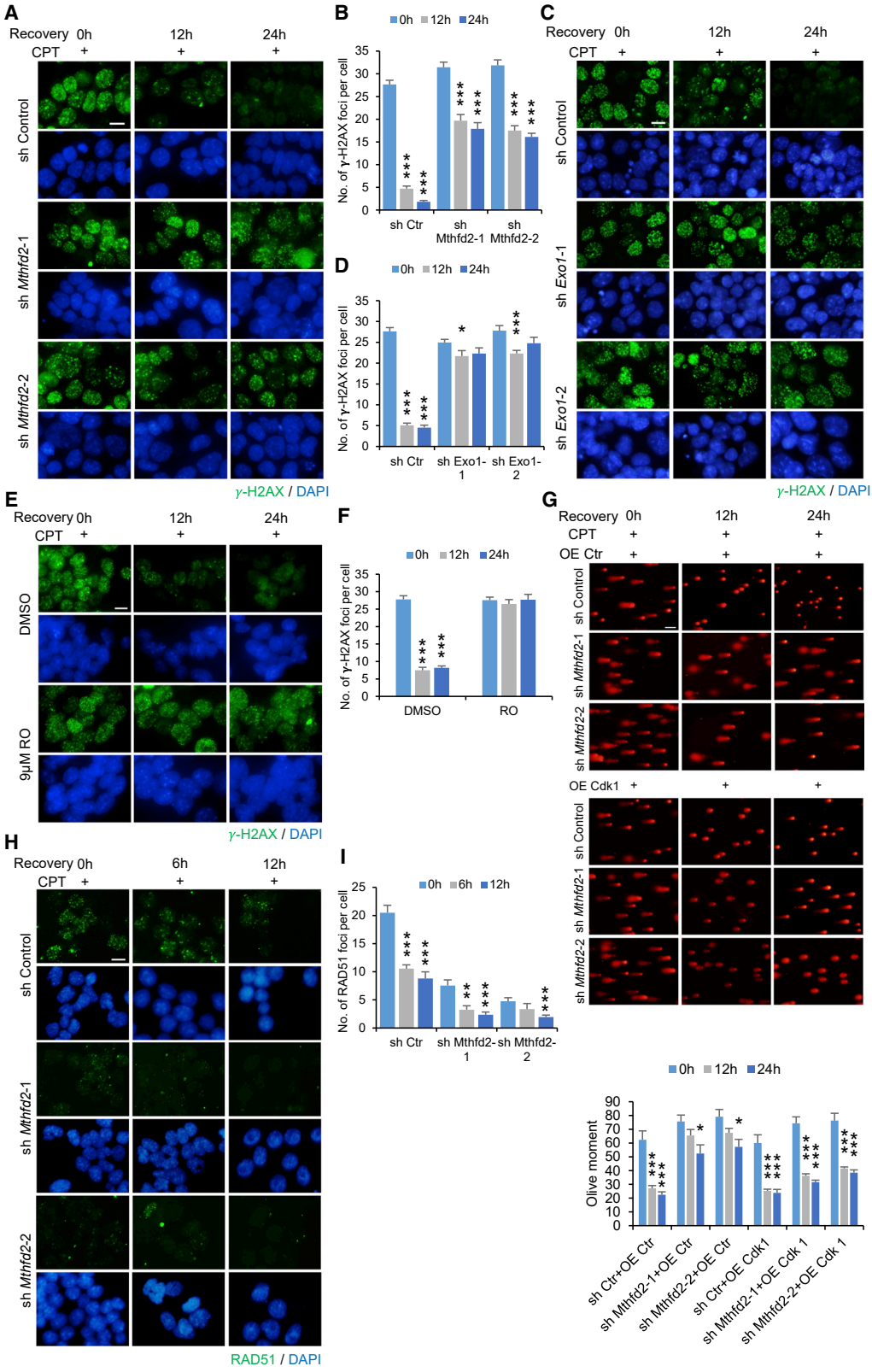

(legend on next page)

Mthfd2 KD mESCs (Figures 7C and 7D). On the other hand, we forced the expression either of *Uqcrc2* or *Cdk1* alone or of *Uqcrc2* and *Cdk1* together in *Mthfd2* KD mESCs (Figures 7E and 7F). Forced co-expression of *Uqcrc2* and *Cdk1* rescued the *Mthfd2* KD-induced changes in cell morphology (Figure 7E) and marker gene expression (Figures 7G and 7H), highlighting that *Mthfd2* regulates pluripotency of PSCs by mediating both mitochondrial function and HR repair.

DISCUSSION

High-quality PSCs can differentiate into various types of cells more stably and efficiently, ensuring application security. Many cellular processes, such as pluripotent gene transcription, epigenetic modification, metabolic remodeling, and genomic integrity were involved in somatic cell reprogramming and cell-fate determination (Doege et al., 2012; Graf et al., 2017; Mathieu and Ruohola-Baker, 2017; Silva et al., 2009), but the mechanisms determining the quality of PSCs remain unclear. In our study, we performed transcriptome analysis combined with an IP-MS assay to reveal that *Mthfd2* regulates both mitochondrial function and HR repair and that *Mthfd2* is a powerful bifunctional regulator for quality of PSCs.

We found that mESCs with inhibited MTHFD2 enzymatic activity retained typical stem cell characteristics. Moreover, the expression of key genes in folate metabolism did not differ between *Mthfd2* KD mESCs and control mESCs (Table S2). These results revealed that *Mthfd2* has non-enzymatic functions in mESCs. *MTHFD2* depletion resulted in an obvious suppression of proliferation and cell death in diverse cancer cell types (Nilsson et al., 2014). In our study, homozygous *Mthfd2* KO mESCs showed compromised proliferation, but there was no significant change in cell proliferation in *Mthfd2* KD mESCs (Table S7). Whether this difference was due to residual MTHFD2 activity in *Mthfd2* KD cells, the activity of other enzymes such as MTHFD2L, or the presence of alternative metabolic pathways that are active in mESCs, is unclear. *MTHFD2* depletion resulted in increased glycolysis in breast cancer cells and lung cancer cells (Koufaris et al., 2016; Nishimura et al., 2019). Our results showed that *Mthfd2* KD induces mitochondrial dysfunction, which suggests that in *Mthfd2*-depleted cells mitochondrial dysfunction may force cells to rely mainly on glycolysis to support the cellular ATP demand. However, we cannot rule out the possibility that increased glycolysis is related to mESC differentiation.

Numerous metabolic enzymes, which are often highly expressed by embryonic or undifferentiated cell types, have previously been found to have non-enzymatic functions in the nucleus (Lincet and Icard, 2015). In mESCs, we identified a role of nuclear *Mthfd2* in preserving HR repair. FILIA physically interacts with PARP1 and stimulates PARP1's enzymatic activity to regulate the DDR (Zhao et al., 2015). Our study indicated that *Mthfd2* plays a role similar to that of *Filia* in the DDR. MTHFD2 directly interacts with CDK1 and affects CDK1's activity to regulate EXO1 phosphorylation, thereby promoting HR repair. The most dangerous form of DNA damage is DSBs that can arise from ROS and others. *Mthfd2* overexpression in the *Drosophila* abdominal fat body significantly reduced ROS levels (Yu et al., 2015), and ROS levels were increased in *Mthfd2* KD mESCs. Hence, *Mthfd2* can maintain genomic integrity by both reducing the levels of ROS and promoting HR repair. Genomic stability is necessary for the survival and function of PSCs (Blanpain et al., 2011) and is also a key aspect of improving the quality of iPSCs (Gonzalez et al., 2013; Jiang et al., 2013). Therefore, *Mthfd2* improves the quality of iPSCs by maintaining genomic stability, thereby ensuring the safety of iPSC applications.

Metabolic transition from OXPHOS to glycolysis is a necessary process for successful reprogramming (Folmes

Figure 6. *Mthfd2* Modulates HR Repair by Regulating EXO1 Phosphorylation

(A and B) IF staining for γ-H2AX in *Mthfd2* KD mESCs at indicated times post CPT treatment. Representative images (A) and quantification of the average number of γ-H2AX foci per cell (B) (n = 50 nuclei) are shown. DAPI was used to indicate the nuclei. Scale bar, 50 μm.

(C and D) IF staining for γ-H2AX in *Exo1* KD mESCs at indicated times post CPT treatment. Representative images (C) and quantification of the average number of γ-H2AX foci per cell (D) (n = 50 nuclei) are shown. DAPI was used to indicate the nuclei. Scale bar, 50 μm.

(E and F) Immunofluorescence staining for γ-H2AX in RO-3306 (RO)-treated mESCs at indicated times post CPT treatment. Representative images (E) and quantification of the average number of γ-H2AX foci per cell (F) (n = 50 nuclei) are shown. DAPI was used to indicate the nuclei. Scale bar, 50 μm.

(G) DNA damage levels in OE *Cdk1-Mthfd2* KD mESCs were evaluated by the comet assay at indicated times post CPT treatment. Representative images (upper panels) and quantification of the mean olive tail moment (lower panel) (n = 50 nuclei) are shown. Scale bar, 100 μm.

(H and I) IF staining for RAD51 in *Mthfd2* KD mESCs at indicated times post CPT treatment. Representative images (H) and quantification of the average number of Rad51 foci per cell (I) (n = 50 nuclei) are shown. DAPI was used to indicate the nuclei. Scale bar, 20 μm.

All data are pooled from three independent experiments (mean ± SEM). *p < 0.05, **p < 0.01, ***p < 0.001 (Student's t test) compared with the control. See also Figure S6.

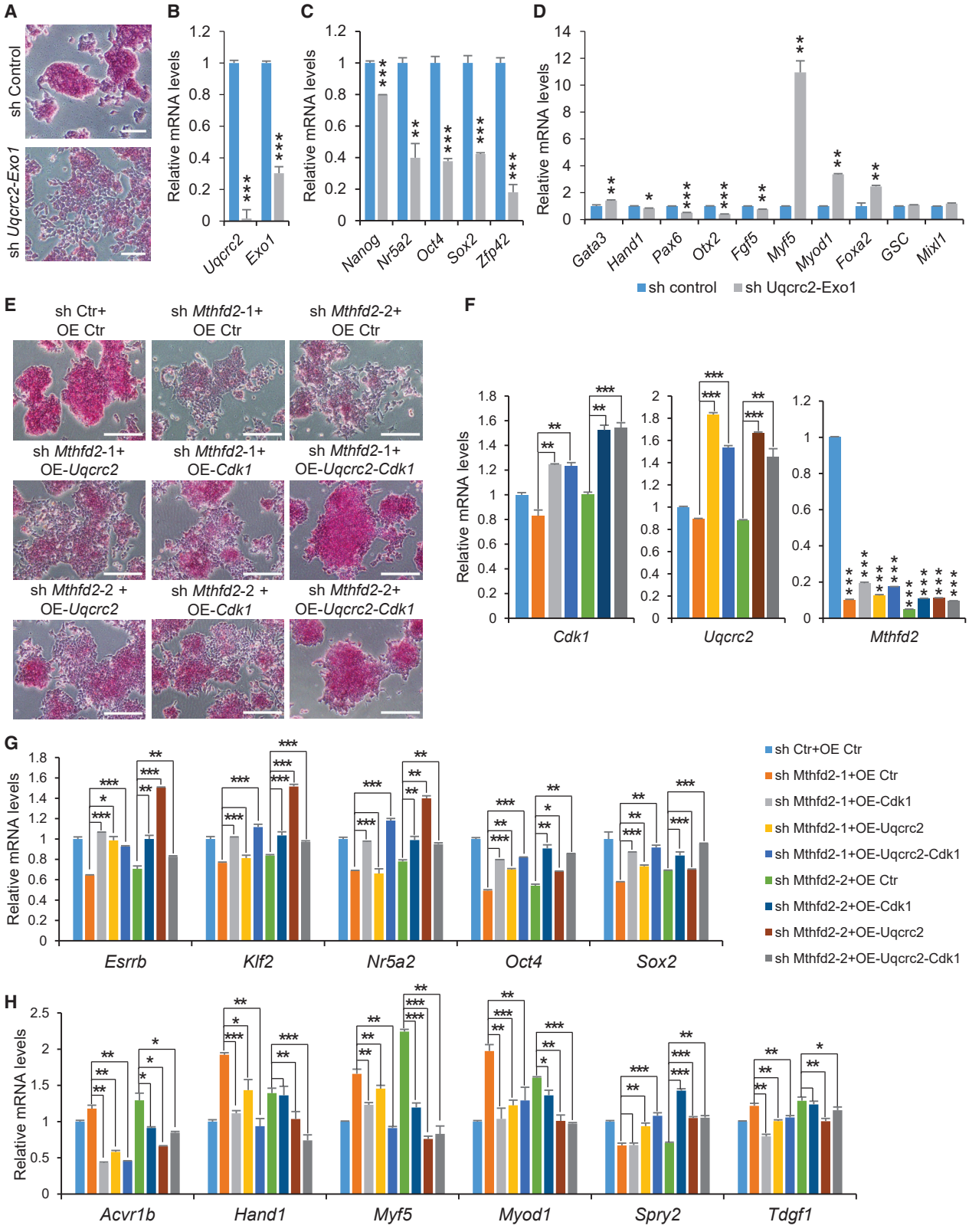

(legend on next page)

et al., 2011; Prigione et al., 2014). However, OXPHOS is also induced and activated at different stages of reprogramming to jointly promote reprogramming (Hawkins et al., 2016; Kida et al., 2015). In our study, overexpression of *Mthfd2* facilitated iPSC induction, suggesting that maintaining active mitochondrial function during reprogramming is beneficial for improving reprogramming efficiency. In PSCs, the metabolic transition from glycolysis to OXPHOS promotes the primed-to-naive state transition (Carbognin et al., 2016). Therefore, in addition to maintaining genomic stability, *Mthfd2* also improves the quality of PSCs by maintaining active OXPHOS. Primed PSCs have lower mitochondrial respiration rates than naive PSCs, which is attributable to a deficiency in ETC complex IV (Zhou et al., 2012). We found that deficiency in ETC complex III also affects the pluripotency state of mESCs. Complex III has two sites, Qo and Qi, to produce ROS. Antimycin A inhibits complex III at the Qi site and increases ROS generation from the Qo site, while it inhibits the Qo site and reduces ROS production (Chen et al., 2003; Demin et al., 1998; Muller et al., 2002). Therefore, *Mthfd2* or *Uqcrc2* depletion may lead to increased ROS production by inhibiting the Qi site instead of the Qo site. MTHFD2 interacts with UQCRC2 to maintain active mitochondrial function, but the interaction is not direct and is mediated by other factors that need further study.

Finally, *Mthfd2* was highly expressed in high-quality iPSCs, and OSKM2 iPSCs were able to develop into viable offspring via tetraploid complementation. The tetraploid complementation assay is the most stringent criterion for assessing the developmental potential of non-human PSCs. Therefore, establishing a fast and effective method to evaluate the pluripotent state of human PSCs is necessary. Moreover, the PSCs of domestic animals such as porcine, bovine, and ovine are still unable to produce chimeras. MTHFD2 is a highly conserved protein between mice and human or domestic animals. Hence, our study should provide new insights into cell pluripotency of other species and provide additional methods to enhance and optimize the acquisition and maintenance of high-quality PSCs.

EXPERIMENTAL PROCEDURES

Co-immunoprecipitation

Cell extracts were prepared in lysis buffer (Beyotime) supplemented with protease inhibitor cocktail and phosphatase inhibitor cocktail (Cell Signaling Technology). To reduce the background, we cleaned the cell extracts with mouse or rabbit immunoglobulin G beads before conducting coIP assays. Antibodies were incubated overnight with cell extracts and then bound to Protein-G beads (Roche) following the manufacturer's protocol. Beads were washed extensively in lysis buffer and then boiled in 2× SDS loading buffer before western blotting.

Data and Code Availability

The accession numbers for the RNA-seq data reported in this paper is SRA: SRP149554.

SUPPLEMENTAL INFORMATION

Supplemental Information can be found online at https://doi.org/10.1016/j.stemcr.2020.06.018.

AUTHOR CONTRIBUTIONS

J.H. conceived and supervised the project. J.H. and L.Y. designed the study and wrote the manuscript. L.Y. performed most experiments and result analyses. Y.P. conducted iPSC induction and results analysis. L.Z. and H.Y. performed bioinformatics analysis. M.Z., S.Z., B.W., J.X., and S.C. performed the iPSC chimeric embryo experiment. Y.W., W.Z., and Q.W. designed the primers. Q.Z., J.G., H.L., and Z.C. helped with the GST pull-down assay, N.C. helped with molecular vector construction. H.L. performed the fluorescence-activated cell sorting experiment.

ACKNOWLEDGMENTS

We thank Andras Nagy, Kristina Vintersten, and Marina Gertsenstein (Mount Sinai Hospital) for their support of G4 ESCs; Dr. Shaorong Gao (Tongji University; National Institute of Biological Sciences) for providing the Oct4-GFP mice, and Dr. Shuai Gao (Tongji University; National Institute of Biological Sciences) for Rosa26-M2rtTA Col1a1-tetO-Pou5f1 (TF4) mice. This work was supported by China National Basic Research Program (2016YFA0100202), National Natural Science Foundation of China (31571497, 31601941, 31772601), Plan 111 (B12008), and Research Programs from the State Key Laboratories for

Figure 7. *Mthfd2* Regulates Pluripotency of mESCs by Modulating both Mitochondrial Function and DNA Repair

(A) Representative results of *Uqcrc2-Exo1* KD mESCs with AP staining. Scale bars, 100 μm.

(B) qRT-PCR analysis of mRNA levels of *Uqcrc2* and *Exo1* in *Uqcrc2-Exo1* KD mESCs.

(C and D) qRT-PCR analysis of mRNA levels of pluripotency marker genes (C) and lineage marker genes (D) in *Uqcrc2-Exo1* KD mESCs.

(E) Representative results of OE *Uqcrc2-*, OE *Cdk1-* or co-OE *Uqcrc2*, and *Cdk1-Mthfd2* KD mESCs with AP staining. Scale bars, 200 μm.

(F) qRT-PCR analysis of mRNA levels of *Uqcrc2*, *Cdk1*, and *Mthfd2* in OE *Uqcrc2-*, OE *Cdk1-* or co-OE *Uqcrc2*, and *Cdk1-Mthfd2* KD mESCs.

(G and H) qRT-PCR analysis of mRNA levels of pluripotency marker genes (G) and lineage marker genes (H) in OE *Uqcrc2-*, OE *Cdk1-* or co-OE *Uqcrc2*, and *Cdk1-Mthfd2* KD mESCs.

Data in (B) to (D) and (F) to (H) are pooled from three independent experiments (mean ± SD) relative to EF1-α and the control. *$p < 0.05$, **$p < 0.01$, ***$p < 0.001$ (Student's t test) compared with the control. See also Figure S7.

Agrobiotechnology and College of Biological Sciences (2020SKLAB1-3, 31051378, 10052521-01).

Received: November 10, 2019
Revised: June 18, 2020
Accepted: June 18, 2020
Published: July 16, 2020

REFERENCES

Aguilera-Aguirre, L., Bacsi, A., Saavedra-Molina, A., Kurosky, A., Sur, S., and Boldogh, I. (2009). Mitochondrial dysfunction increases allergic airway inflammation. J. Immunol. *183*, 5379–5387.

Asai, A., Koseki, J., Konno, M., Nishimura, T., Gotoh, N., Satoh, T., Doki, Y., Mori, M., and Ishii, H. (2018). Drug discovery of anticancer drugs targeting methylenetetrahydrofolate dehydrogenase 2. Heliyon *4*, e01021.

Blanpain, C., Mohrin, M., Sotiropoulou, P.A., and Passegue, E. (2011). DNA-damage response in tissue-specific and cancer stem cells. Cell Stem Cell *8*, 16–29.

Boroviak, T., Loos, R., Lombard, P., Okahara, J., Behr, R., Sasaki, E., Nichols, J., Smith, A., and Bertone, P. (2015). Lineage-specific profiling delineates the emergence and progression of naive pluripotency in mammalian embryogenesis. Dev. Cell *35*, 366–382.

Carbognin, E., Betto, R.M., Soriano, M.E., Smith, A.G., and Martello, G. (2016). Stat3 promotes mitochondrial transcription and oxidative respiration during maintenance and induction of naive pluripotency. EMBO J. *35*, 618–634.

Chen, K., Long, Q., Wang, T., Zhao, D., Zhou, Y., Qi, J., Wu, Y., Li, S., Chen, C., Zeng, X., et al. (2016). Gadd45a is a heterochromatin relaxer that enhances iPS cell generation. EMBO Rep. *17*, 1641–1656.

Chen, Q., Vazquez, E.J., Moghaddas, S., Hoppel, C.L., and Lesnefsky, E.J. (2003). Production of reactive oxygen species by mitochondria: central role of complex III. J. Biol. Chem. *278*, 36027–36031.

Crofts, A.R. (2004). The cytochrome bc1 complex: function in the context of structure. Annu. Rev. Physiol. *66*, 689–733.

Demin, O.V., Kholodenko, B.N., and Skulachev, V.P. (1998). A model of O2.-generation in the complex III of the electron transport chain. Mol. Cell. Biochem. *184*, 21–33.

Desmarais, J.A., Unger, C., Damjanov, I., Meuth, M., and Andrews, P. (2016). Apoptosis and failure of checkpoint kinase 1 activation in human induced pluripotent stem cells under replication stress. Stem Cell Res. Ther. *7*, 17.

Di Pietro, E., Sirois, J., Tremblay, M.L., and MacKenzie, R.E. (2002). Mitochondrial NAD-dependent methylenetetrahydrofolate dehydrogenase-methenyltetrahydrofolate cyclohydrolase is essential for embryonic development. Mol. Cell. Biol. *22*, 4158–4166.

Doege, C.A., Inoue, K., Yamashita, T., Rhee, D.B., Travis, S., Fujita, R., Guarnieri, P., Bhagat, G., Vanti, W.B., Shih, A., et al. (2012). Early-stage epigenetic modification during somatic cell reprogramming by Parp1 and Tet2. Nature *488*, 652–655.

Evans, M.J., and Kaufman, M.H. (1981). Establishment in culture of pluripotential cells from mouse embryos. Nature *292*, 154–156.

Feng, B., Jiang, J., Kraus, P., Ng, J.-H., Heng, J.-C.D., Chan, Y.-S., Yaw, L.-P., Zhang, W., Loh, Y.-H., Han, J., et al. (2009). Reprogramming of fibroblasts into induced pluripotent stem cells with orphan nuclear receptor Esrrb. Nat. Cell Biol. *11*, 197–203.

Folmes, C.D., Nelson, T.J., Martinez-Fernandez, A., Arrell, D.K., Lindor, J.Z., Dzeja, P.P., Ikeda, Y., Perez-Terzic, C., and Terzic, A. (2011). Somatic oxidative bioenergetics transitions into pluripotency-dependent glycolysis to facilitate nuclear reprogramming. Cell Metab. *14*, 264–271.

Gao, S., Wang, Z.L., Di, K.Q., Chang, G., Tao, L., An, L., Wu, F.J., Xu, J.Q., Liu, Y.W., Wu, Z.H., et al. (2013). Melatonin improves the reprogramming efficiency of murine-induced pluripotent stem cells using a secondary inducible system. J. Pineal Res. *55*, 31–39.

Gonzalez, F., Georgieva, D., Vanoli, F., Shi, Z.D., Stadtfeld, M., Ludwig, T., Jasin, M., and Huangfu, D. (2013). Homologous recombination DNA repair genes play a critical role in reprogramming to a pluripotent state. Cell Rep. *3*, 651–660.

Graf, U., Casanova, E.A., Wyck, S., Dalcher, D., Gatti, M., Vollenweider, E., Okoniewski, M.J., Weber, F.A., Patel, S.S., Schmid, M.W., et al. (2017). Pramel7 mediates ground-state pluripotency through proteasomal-epigenetic combined pathways. Nat. Cell Biol. *19*, 763–773.

Gustafsson Sheppard, N., Jarl, L., Mahadessian, D., Strittmatter, L., Schmidt, A., Madhusudan, N., Tegner, J., Lundberg, E.K., Asplund, A., Jain, M., et al. (2015). The folate-coupled enzyme MTHFD2 is a nuclear protein and promotes cell proliferation. Sci. Rep. *5*, 15029.

Han, J., Yuan, P., Yang, H., Zhang, J., Soh, B.S., Li, P., Lim, S.L., Cao, S., Tay, J., Orlov, Y.L., et al. (2010). Tbx3 improves the germ-line competency of induced pluripotent stem cells. Nature *463*, 1096–1100.

Hatefi, Y. (1985). The mitochondrial electron transport and oxidative phosphorylation system. Annu. Rev. Biochem. *54*, 1015–1069.

Hawkins, K.E., Joy, S., Delhove, J.M., Kotiadis, V.N., Fernandez, E., Fitzpatrick, L.M., Whiteford, J.R., King, P.J., Bolanos, J.P., Duchen, M.R., et al. (2016). NRF2 orchestrates the metabolic shift during induced pluripotent stem cell reprogramming. Cell Rep. *14*, 1883–1891.

Heng, J.C., Feng, B., Han, J., Jiang, J., Kraus, P., Ng, J.H., Orlov, Y.L., Huss, M., Yang, L., Lufkin, T., et al. (2010). The nuclear receptor Nr5a2 can replace Oct4 in the reprogramming of murine somatic cells to pluripotent cells. Cell Stem Cell *6*, 167–174.

Hsiang, Y.H., Lihou, M.G., and Liu, L.F. (1989). Arrest of replication forks by drug-stabilized topoisomerase I-DNA cleavable complexes as a mechanism of cell killing by camptothecin. Cancer Res. *49*, 5077–5082.

Huang, Y., Osorno, R., Tsakiridis, A., and Wilson, V. (2012). In vivo differentiation potential of epiblast stem cells revealed by chimeric embryo formation. Cell Rep. *2*, 1571–1578.

Jackson, S.P. (2002). Sensing and repairing DNA double-strand breaks. Carcinogenesis *23*, 687–696.

Jiang, J., Lv, W., Ye, X., Wang, L., Zhang, M., Yang, H., Okuka, M., Zhou, C., Zhang, X., Liu, L., et al. (2013). Zscan4 promotes genomic stability during reprogramming and dramatically improves the quality of iPS cells as demonstrated by tetraploid complementation. Cell Res. *23*, 92–106.

Khacho, M., Clark, A., Svoboda, D.S., Azzi, J., MacLaurin, J.G., Meghaizel, C., Sesaki, H., Lagace, D.C., Germain, M., Harper, M.E., et al. (2016). Mitochondrial dynamics impacts stem cell identity and fate decisions by regulating a nuclear transcriptional Program. Cell Stem Cell *19*, 232–247.

Kida, Y.S., Kawamura, T., Wei, Z., Sogo, T., Jacinto, S., Shigeno, A., Kushige, H., Yoshihara, E., Liddle, C., Ecker, J.R., et al. (2015). ERRs mediate a metabolic switch required for somatic cell reprogramming to pluripotency. Cell Stem Cell *16*, 547–555.

Koufaris, C., Gallage, S., Yang, T., Lau, C.H., Valbuena, G.N., and Keun, H.C. (2016). Suppression of MTHFD2 in MCF-7 breast cancer cells increases glycolysis, dependency on exogenous Glycine, and sensitivity to folate depletion. J. Proteome Res. *15*, 2618–2625.

Lee, J.Y., Kim, D.K., Ko, J.J., Kim, K.P., and Park, K.S. (2016). Rad51 regulates reprogramming efficiency through DNA repair pathway. Dev. Reprod. *20*, 163–169.

Li, M., He, Y., Dubois, W., Wu, X., Shi, J., and Huang, J. (2012). Distinct regulatory mechanisms and functions for p53-activated and p53-repressed DNA damage response genes in embryonic stem cells. Mol. Cell *46*, 30–42.

Lin, H., Huang, B., Wang, H., Liu, X., Hong, Y., Qiu, S., and Zheng, J. (2018). MTHFD2 overexpression predicts poor prognosis in renal cell carcinoma and is associated with cell proliferation and vimentin-modulated migration and invasion. Cell. Physiol. Biochem. *51*, 991–1000.

Lin, T., Chao, C., Saito, S., Mazur, S.J., Murphy, M.E., Appella, E., and Xu, Y. (2005). p53 induces differentiation of mouse embryonic stem cells by suppressing Nanog expression. Nat. Cell Biol. *7*, 165–171.

Lincet, H., and Icard, P. (2015). How do glycolytic enzymes favour cancer cell proliferation by nonmetabolic functions? Oncogene *34*, 3751–3759.

Liu, F., Liu, Y., He, C., Tao, L., He, X., Song, H., and Zhang, G. (2014a). Increased MTHFD2 expression is associated with poor prognosis in breast cancer. Tumour Biol. *35*, 8685–8690.

Liu, J.C., Guan, X., Ryan, J.A., Rivera, A.G., Mock, C., Agrawal, V., Letai, A., Lerou, P.H., and Lahav, G. (2013). High mitochondrial priming sensitizes hESCs to DNA-damage-induced apoptosis. Cell Stem Cell *13*, 483–491.

Liu, K., Wang, F., Ye, X., Wang, L., Yang, J., Zhang, J., and Liu, L. (2014b). KSR-based medium improves the generation of high-quality mouse iPS cells. PLoS One *9*, e105309.

Mathieu, J., and Ruohola-Baker, H. (2017). Metabolic remodeling during the loss and acquisition of pluripotency. Development *144*, 541–551.

Mitchell, P. (1975). Protonmotive redox mechanism of the cytochrome b-c1 complex in the respiratory chain: protonmotive ubiquinone cycle. FEBS Lett. *56*, 1–6.

Miyake, N., Yano, S., Sakai, C., Hatakeyama, H., Matsushima, Y., Shiina, M., Watanabe, Y., Bartley, J., Abdenur, J.E., Wang, R.Y., et al. (2013). Mitochondrial complex III deficiency caused by a homozygous UQCRC2 mutation presenting with neonatal-onset recurrent metabolic decompensation. Hum. Mutat. *34*, 446–452.

Muller, F., Crofts, A.R., and Kramer, D.M. (2002). Multiple Q-cycle bypass reactions at the Qo site of the cytochrome bc1 complex. Biochemistry *41*, 7866–7874.

Nichols, J., and Smith, A. (2009). Naive and primed pluripotent states. Cell Stem Cell *4*, 487–492.

Nilsson, R., Jain, M., Madhusudhan, N., Sheppard, N.G., Strittmatter, L., Kampf, C., Huang, J., Asplund, A., and Mootha, V.K. (2014). Metabolic enzyme expression highlights a key role for MTHFD2 and the mitochondrial folate pathway in cancer. Nat. Commun. *5*, 3128.

Nishimura, T., Nakata, A., Chen, X., Nishi, K., Meguro-Horike, M., Sasaki, S., Kita, K., Horike, S.I., Saitoh, K., Kato, K., et al. (2019). Cancer stem-like properties and gefitinib resistance are dependent on purine synthetic metabolism mediated by the mitochondrial enzyme MTHFD2. Oncogene *38*, 2464–2481.

Pei, Y., Yue, L., Zhang, W., Wang, Y., Wen, B., Zhong, L., Xiang, J., Li, J., Zhang, S., Wang, H., et al. (2015). Improvement in mouse iPSC induction by Rab32 reveals the importance of lipid metabolism during reprogramming. Sci. Rep. *5*, 16539.

Pikman, Y., Puissant, A., Alexe, G., Furman, A., Chen, L.M., Frumm, S.M., Ross, L., Fenouille, N., Bassil, C.F., Lewis, C.A., et al. (2016). Targeting MTHFD2 in acute myeloid leukemia. J. Exp. Med. *213*, 1285–1306.

Prigione, A., Rohwer, N., Hoffmann, S., Mlody, B., Drews, K., Bukowiecki, R., Blumlein, K., Wanker, E.E., Ralser, M., Cramer, T., et al. (2014). HIF1alpha modulates cell fate reprogramming through early glycolytic shift and upregulation of PDK1-3 and PKM2. Stem Cells *32*, 364–376.

Rogakou, E.P., Pilch, D.R., Orr, A.H., Ivanova, V.S., and Bonner, W.M. (1998). DNA double-stranded breaks induce histone H2AX phosphorylation on serine 139. J. Biol. Chem. *273*, 5858–5868.

Ryu, J.M., Lee, H.J., Jung, Y.H., Lee, K.H., Kim, D.I., Kim, J.Y., Ko, S.H., Choi, G.E., Chai, , II, Song, E.J., et al. (2015). Regulation of stem cell fate by ROS-mediated alteration of metabolism. Int. J. Stem Cells *8*, 24–35.

Schaetzlein, S., Kodandaramireddy, N.R., Ju, Z., Lechel, A., Stepczynska, A., Lilli, D.R., Clark, A.B., Rudolph, C., Kuhnel, F., Wei, K., et al. (2007). Exonuclease-1 deletion impairs DNA damage signaling and prolongs lifespan of telomere-dysfunctional mice. Cell *130*, 863–877.

Shyh-Chang, N., and Daley, G.Q. (2015). Metabolic switches linked to pluripotency and embryonic stem cell differentiation. Cell Metab. *21*, 349–350.

Silva, J., Nichols, J., Theunissen, T.W., Guo, G., van Oosten, A.L., Barrandon, O., Wray, J., Yamanaka, S., Chambers, I., and Smith, A. (2009). Nanog is the gateway to the pluripotent ground state. Cell *138*, 722–737.

Sukumar, M., Liu, J., Mehta, G.U., Patel, S.J., Roychoudhuri, R., Crompton, J.G., Klebanoff, C.A., Ji, Y., Li, P., Yu, Z., et al. (2016). Mitochondrial membrane potential identifies cells with enhanced stemness for cellular therapy. Cell Metab. *23*, 63–76.

Takahashi, K., and Yamanaka, S. (2006). Induction of pluripotent stem cells from mouse embryonic and adult fibroblast cultures by defined factors. Cell *126*, 663–676.

Takashima, Y., Guo, G., Loos, R., Nichols, J., Ficz, G., Krueger, F., Oxley, D., Santos, F., Clarke, J., Mansfield, W., et al. (2014). Resetting transcription factor control circuitry toward ground-state pluripotency in human. Cell *158*, 1254–1269.

Tesar, P.J., Chenoweth, J.G., Brook, F.A., Davies, T.J., Evans, E.P., Mack, D.L., Gardner, R.L., and McKay, R.D. (2007). New cell lines from mouse epiblast share defining features with human embryonic stem cells. Nature *448*, 196–199.

Tibbetts, A.S., and Appling, D.R. (2010). Compartmentalization of Mammalian folate-mediated one-carbon metabolism. Annu. Rev. Nutr. *30*, 57–81.

Tichy, E.D., Pillai, R., Deng, L., Liang, L., Tischfield, J., Schwemberger, S.J., Babcock, G.F., and Stambrook, P.J. (2010). Mouse embryonic stem cells, but not somatic cells, predominantly use homologous recombination to repair double-strand DNA breaks. Stem Cells Dev. *19*, 1699–1711.

Tomimatsu, N., Mukherjee, B., Catherine Hardebeck, M., Ilcheva, M., Vanessa Camacho, C., Louise Harris, J., Porteus, M., Llorente, B., Khanna, K.K., and Burma, S. (2014). Phosphorylation of EXO1 by CDKs 1 and 2 regulates DNA end resection and repair pathway choice. Nat. Commun. *5*, 3561.

Weissbein, U., Benvenisty, N., and Ben-David, U. (2014). Quality control: genome maintenance in pluripotent stem cells. J. Cell Biol. *204*, 153–163.

Xiang, J., Cao, S., Zhong, L., Wang, H., Pei, Y., Wei, Q., Wen, B., Mu, H., Zhang, S., Yue, L., et al. (2018). Pluripotent stem cells secrete Activin A to improve their epiblast competency after injection into recipient embryos. Protein Cell *9*, 717–728.

Yoshihara, M., Hayashizaki, Y., and Murakawa, Y. (2017). Genomic instability of iPSCs: challenges towards their clinical applications. Stem Cell Rev. Rep. *13*, 7–16.

Yu, S., Jang, Y., Paik, D., Lee, E., and Park, J.J. (2015). Nmdmc overexpression extends Drosophila lifespan and reduces levels of mitochondrial reactive oxygen species. Biochem. Biophys. Res. Commun. *465*, 845–850.

Zhang, J., Ratanasirintrawoot, S., Chandrasekaran, S., Wu, Z., Ficarro, S.B., Yu, C., Ross, C.A., Cacchiarelli, D., Xia, Q., Seligson, M., et al. (2016). LIN28 regulates stem cell metabolism and conversion to primed pluripotency. Cell Stem Cell *19*, 66–80.

Zhang, J., Tam, W.L., Tong, G.Q., Wu, Q., Chan, H.Y., Soh, B.S., Lou, Y., Yang, J., Ma, Y., Chai, L., et al. (2006). Sall4 modulates embryonic stem cell pluripotency and early embryonic development by the transcriptional regulation of Pou5f1. Nat. Cell Biol. *8*, 1114–1123.

Zhang, Y., Cui, P., Li, Y., Feng, G., Tong, M., Guo, L., Li, T., Liu, L., Li, W., and Zhou, Q. (2018). Mitochondrially produced ATP affects stem cell pluripotency via Actl6a-mediated histone acetylation. FASEB J. *32*, 1891–1902.

Zhao, B., Zhang, W.D., Duan, Y.L., Lu, Y.Q., Cun, Y.X., Li, C.H., Guo, K., Nie, W.H., Li, L., Zhang, R., et al. (2015). Filia is an ESC-specific regulator of DNA damage response and safeguards genomic stability. Cell Stem Cell *16*, 684–698.

Zhao, X.Y., Li, W., Lv, Z., Liu, L., Tong, M., Hai, T., Hao, J., Guo, C.L., Ma, Q.W., Wang, L., et al. (2009). iPS cells produce viable mice through tetraploid complementation. Nature *461*, 86–90.

Zhong, X., Cui, P., Cai, Y., Wang, L., He, X., Long, P., Lu, K., Yan, R., Zhang, Y., Pan, X., et al. (2019). Mitochondrial dynamics is critical for the Full pluripotency and embryonic developmental potential of pluripotent stem cells. Cell Metab. *29*, 979–992.e4.

Zhou, G., Meng, S., Li, Y., Ghebre, Y.T., and Cooke, J.P. (2016). Optimal ROS signaling is critical for nuclear reprogramming. Cell Rep. *15*, 919–925.

Zhou, W., Choi, M., Margineantu, D., Margaretha, L., Hesson, J., Cavanaugh, C., Blau, C.A., Horwitz, M.S., Hockenbery, D., Ware, C., et al. (2012). HIF1alpha induced switch from bivalent to exclusively glycolytic metabolism during ESC-to-EpiSC/hESC transition. EMBO J. *31*, 2103–2116.